Observation and Investigation of 14 Wide Common Proper Motion Doubles in the Washington Double Star Catalog

Ryan Caputo, Brandon Bonifacio, Sahana Datar, Sebastian Dehnadi, Lian E, Talia Green, Krithi Koodli, Elias Koubaa, Calla Marchetti, Sujay Nair, Greta Olson, Quinn Perian, Gurmehar Singh, Cindy Wang, Paige Yeung, Peyton Robertson, Elliott Chalcraft, Kalée Tock

Stanford Online High School, Stanford, California

Abstract: As a class-wide introduction to double star research, we investigated and measured 14 physical systems with separations between 6" and 20" from the Washington Double Star Catalog. Between 8 and 12 images of each system were reduced using AstroImageJ to extract position angles and separations that are current for 2020.0. The resulting measurements are reported here and are plotted along with each system's historical data. Along with these plots, each system's measurements in Gaia Data Release 2 were analyzed to assess the probability that the two stars in the system might have a gravitational relationship.

Introduction

Targets for this study were selected and imaged by the course TA, Ryan Caputo. The targets have component stars of similar brightness (delta magnitude < 3) and separations of approximately 10". These criteria ensure that the stars can be resolved easily and measured unambiguously. Moreover, the targets all have similar parallax and proper motions (PMs). The similarity of the component PMs is assessed by taking the ratio of the magnitude of the proper motion difference vector to the magnitude of the longer proper motion vector between the two component stars. This ratio is called the rPM, and double star systems are considered to have common proper motion if its value is smaller than 0.2 (Harshaw, 2016). According to this criterion, all of the systems in Table 1 have common proper motion. Two of them also have orbital solutions in the Washington Double Star Catalog.

As is evident from Table 1, STF1050AB and STF1124AB have parallaxes below 5 milliarcseconds (mas), which causes the fractional parallax uncertainty for these systems to be relatively high. This leads to a large uncertainty in the distances of these systems, where distance is calculated by inverting the parallax. In general, parallax measurements below 5 mas must be treated with caution, as such low values approach the limits of the instrument's sensitivity, and some of the systematic errors associated with Gaia DR2 instrumentation are not fully understood (Luri et. al., 2018).

Instruments Used

For 13 of the 14 systems, images were obtained using a 6-inch aperture classical Cassegrain telescope. The methodology is as described in Caputo 2019. There were no filters used. The camera and telescope combination yields a pixel scale of approximately 0.4" per pixel, giving excellent sampling for seeing-limited measurements. Guiding was employed for longer exposures to improve tracking accuracy. The remaining system, STF1547AB, was imaged using the Las Cumbres Observatory 0.4m robotic telescope.

Measurements

The position angle and separation of each system was measured using AstroImageJ. The measurements are shown in Table 2.

Current measurements in the context of previous measurements

Previous measurements for each system were requested from the US Naval Observatory. These data are plotted along with the measurements above for each system in Figure 1. Outlying data points more than 3

(Text continues on page 175)

System	Parallax of Primary (mas)	Parallax of Secondary (mas)	Proper Motion of Primary (mas/yr)	Proper Motion of Secondary (mas/yr)	rPM
STF1188	11.6 ± 0.06	11.5 ± 0.05	(-9.8 ± 0.10, 12.7 ± 0.06)	(-9.6 ± 0.08, 10.2 ± 0.06)	0.162
STF 427	6.4 ± 0.08	6.4 ± 0.2	(20.4 ± 0.12, -38.0 ± 0.08)	(22.0 ± 0.23, -41.0 ± 0.1)	0.074
STF 872AB	12.9 ± 0.05	12.9 ± 0.04	(-65.5 ± 0.09, 4.6 ± 0.07)	(-64.0 ± 0.09, 1.72 ± 0.07)	0.050
STF 612AB	33.7 ± 0.05	33.8 ± 0.05	(248.1 ± 0.08, -202.0 ± 0.06)	(246.1 ± 0.08, -197.6 ± 0.06)	0.015
COU 91AB	56.0 ± 0.05	55.9 ± 0.20	(-296.7 ± 0.07, -355.8 ± 0.04)	(-270.4 ± 0.31, -365.0 ± 0.16)	0.060
STF1219	19.6 ± 0.05	19.7 ± 0.05	(13.9 ± 0.08, -19.1 ± 0.06)	(16.2 ± 0.09, -21.3 ± 0.06)	0.119
STF1246	12.0 ± 0.04	12.0 ± 0.03	(-17.3 ± 0.08, -7.3 ± 0.05)	(-18.2 ± 0.07, -8.4 ± 0.05)	0.072
STT 195AB	11.0 ± 0.09	11.1 ± 0.07	(-51.04 ± 0.13, 19.2 ± 0.08)	(-41.0 ± 0.12, 19.0 ± 0.08)	0.184
STF1050AB	4.2 ± 0.05	4.2 ± 0.06	(1.7 ± 0.08, -27.4 ± 0.06)	(2.26 ± 0.09, -27.5 ± 0.07)	0.021
STF1124AB	2.9 ± 0.07	2.9 ± 0.05	(-12.6 ± 0.14, -1.3 ± 0.10)	(-11.9 ± 0.11, -1.3 ± 0.07)	0.056
STF 443AB (ORB)	41.8 ± 0.04	41.4 ± 0.05	(598.0 ± 0.08, -1243.9 ± 0.06)	(588.7 ± 0.01, -1262.0 ± 0.09)	0.0147
STF1308	8.0 ± 0.05	8.0 ± 0.12	(-71.4 ± 0.10, 3.1 ± 0.10)	(-71.8 ± 0.21, 4.8 ± 0.19)	0.023
STF1547AB (ORB)	42.3 ± 0.08	42.3 ± 0.06	(-330.3 ± 0.43, -190.1 ± 0.12)	(-315.6 ± 0.11, -181.3 ± 0.07)	0.045
HJ 540	5.6 ± 0.03	5.8 ± 0.04	(-46.2 ± 0.02, 20.2 ± 0.03)	(-46.9 ± 0.03, 20.8 ± 0.05)	0.018

Note: Systems with (ORB) following the designation have an existing orbital solution in the Washington Double Star Catalog.

Table 1: Parallax and proper motion data for each system, including the proper motion ratio (rPM) calculated as the ratio of the PM difference vector magnitude to the magnitude of the longer of the component PM vectors. All of these systems have rPM lower than 0.2, indicating common proper motion.

System	Date	Number of Images	Position Angle (°)	Standard Error on PA	Separation (")	Standard Error on Sep
STF1188	2020.11	12	201.34	0.016	16.38	0.015
STF 427	2020.03	10	206.06	0.295	7.16	0.121
STF 872AB	2020.01	10	215.86	0.076	11.44	0.018
STF 612AB	2020.03	10	200.07	0.021	16.09	0.008
COU 91AB	2020.03	10	143.60	0.022	10.75	0.007
STF1219	2020.03	10	82.40	0.174	12.15	0.056
STF1246	2020.03	10	116.04	0.029	10.58	0.009
STT 195AB	2020.03	10	138.41	0.056	9.83	0.012
STF1050AB	2020.01	9	20.58	0.041	19.37	0.013
STF1124AB	2020.01	10	325.32	0.312	19.34	0.130
STF 443AB	2020.03	10	56.17	0.053	6.74	0.010
STF1308	2020.01	10	84.49	0.043	10.54	0.010
STF1547AB	2020.05	10	330.43	0.081	15.68	0.013
HJ 540	2020.01	9	211.40	0.022	8.90	0.007

Table 2. Measurements of 14 double stars made in January, 2020.

standard deviations from the mean were removed from each plot, and historical data points were corrected for the precession of Earth's axis since the time of each measurement. Note that the plots of Figure 1 are chronological, because each measurement is colored according to the date on which it was made. Specifically, darker points are more recent. A common trend is that the lighter-colored points are more scattered, indicating relatively higher noise in the earlier measurements. In each case, the historical measurements are plotted as circles; the student's measurement, by contrast, is a green square with an x. The plots are labeled with the discoverer code of the system as well as the name of the student who made the measurement.

(Continued on page 178)

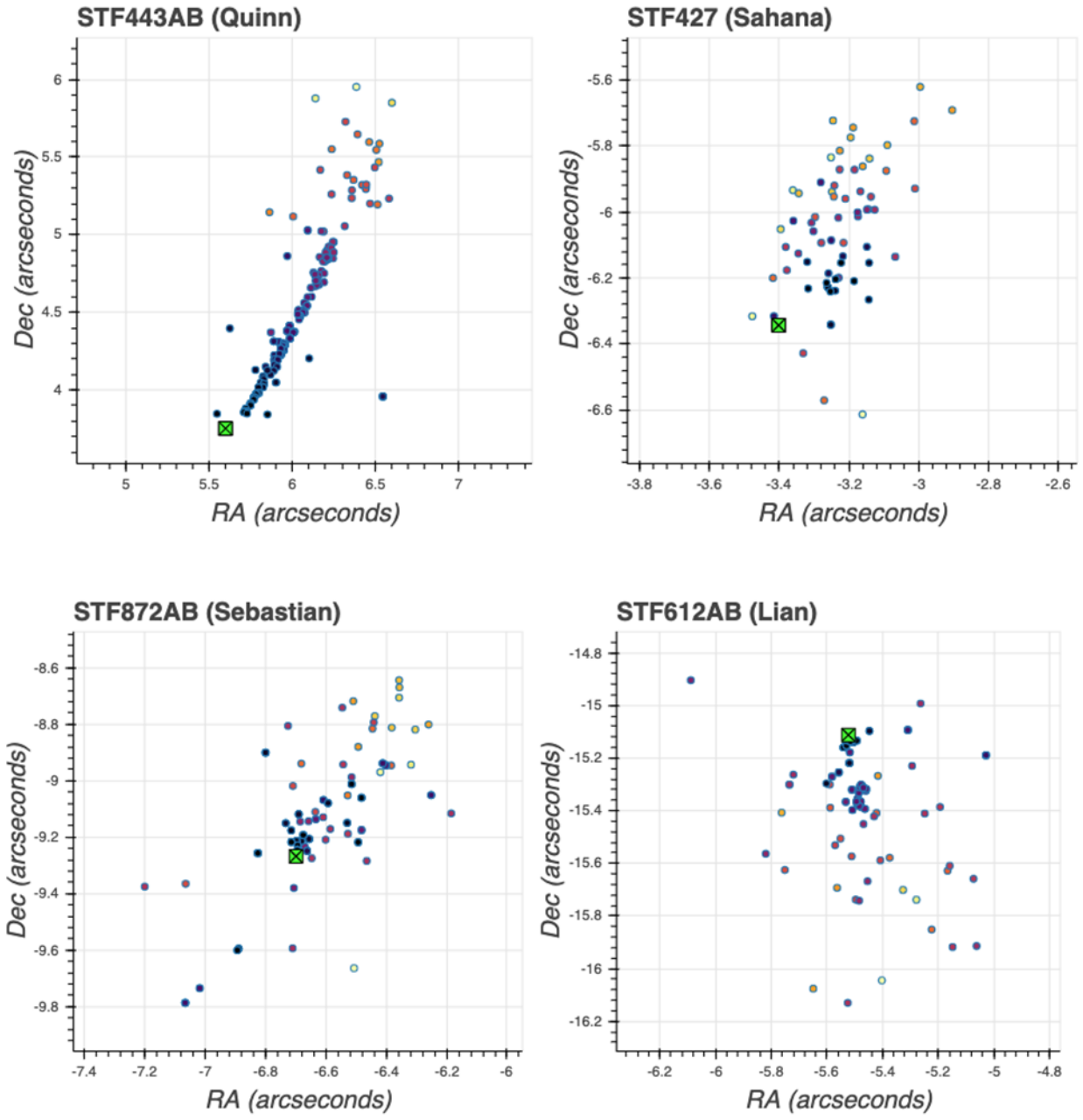

Figure 1: Measurements of each system in the context of historical data, with more recent measurements colored darker, and the measurement reported in this paper shown as a green square with an x through it. (figure continues on next page)

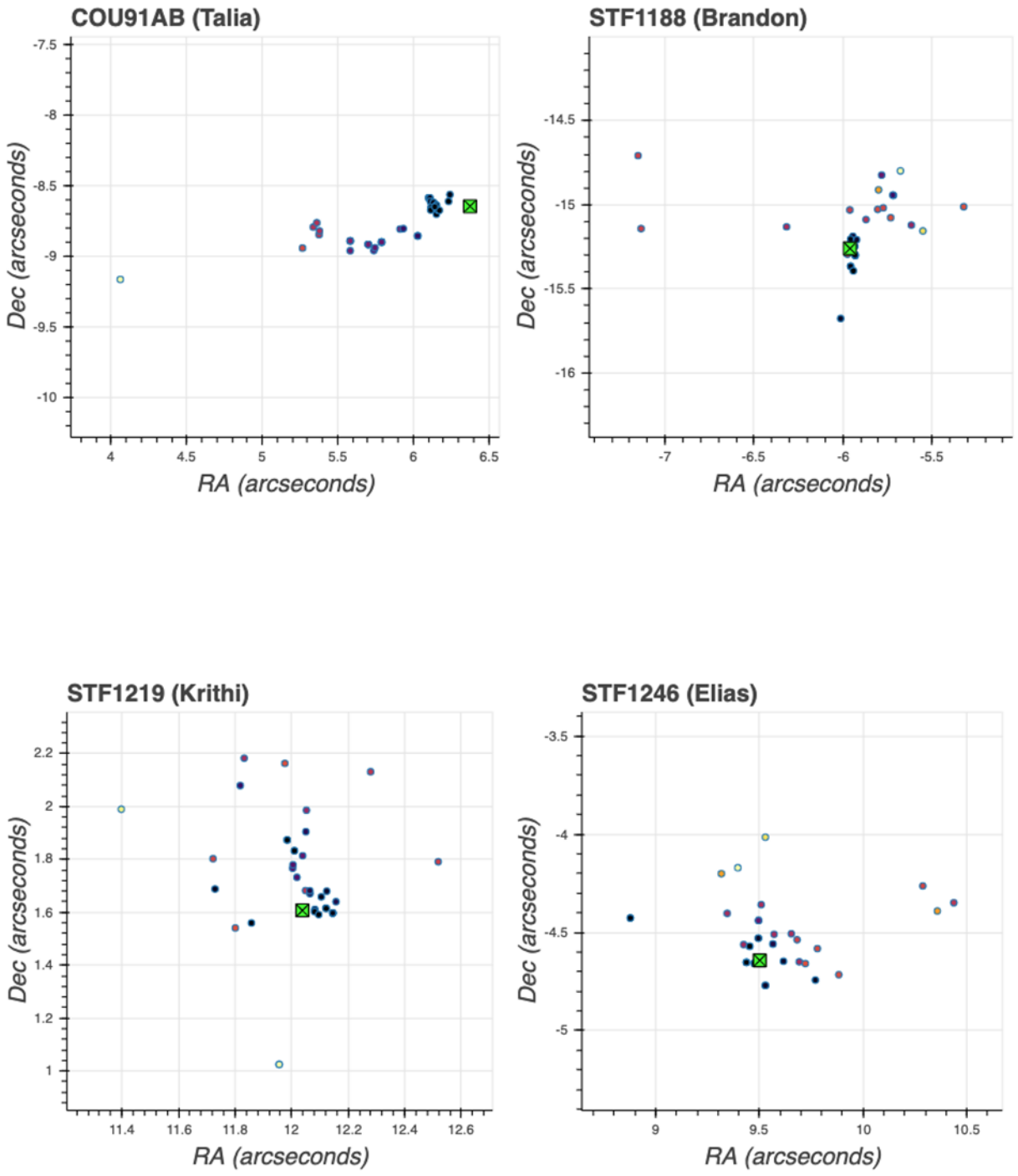

Figure 1 (continued). Measurements of each system in the context of historical data, with more recent measurements colored darker, and the measurement reported in this paper shown as a green square with an x through it. *(figure continues on next page)*

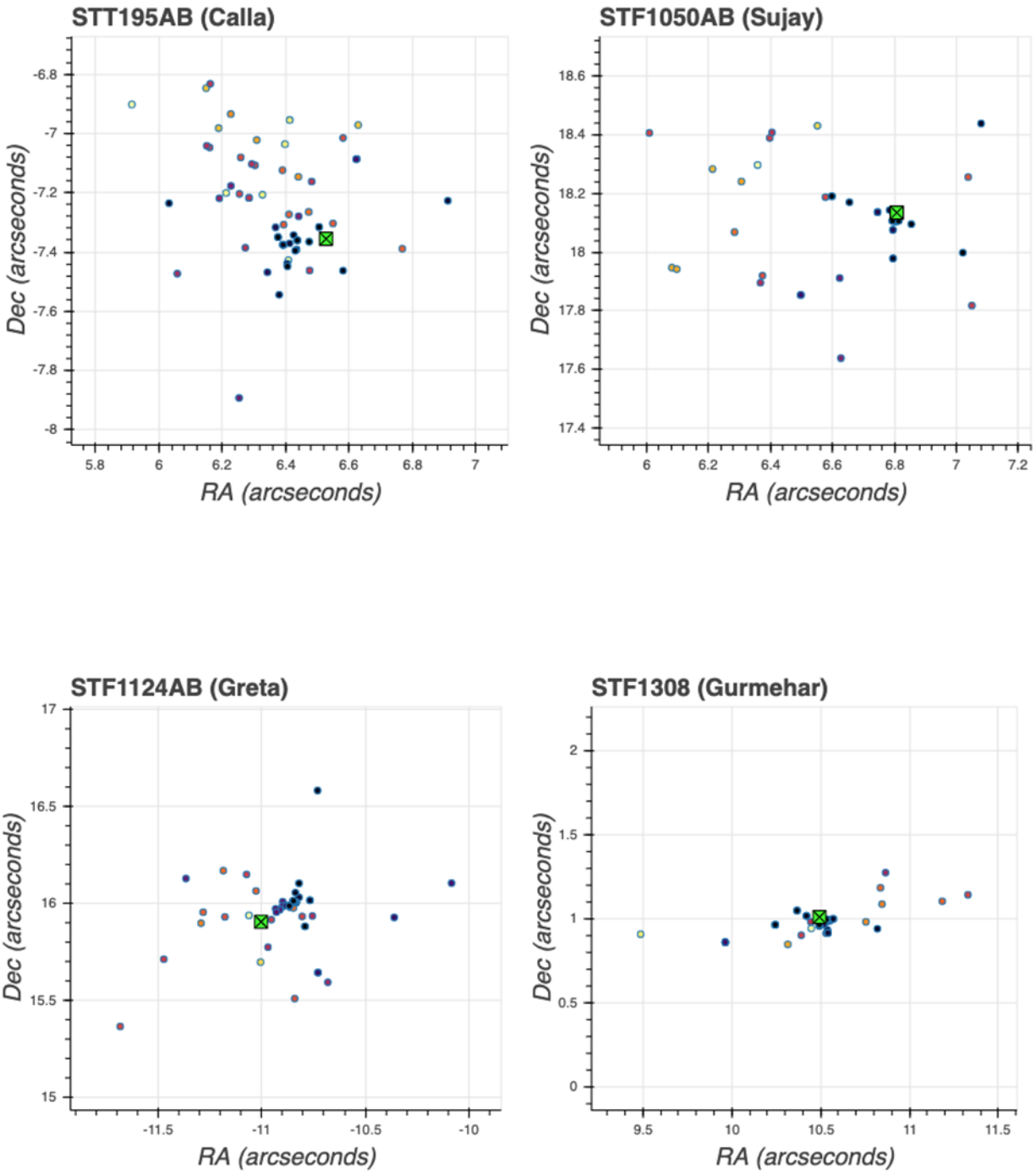

Figure 1 (continued). Measurements of each system in the context of historical data, with more recent measurements colored darker, and the measurement reported in this paper shown as a green square with an x through it. (figure concludes on next page)

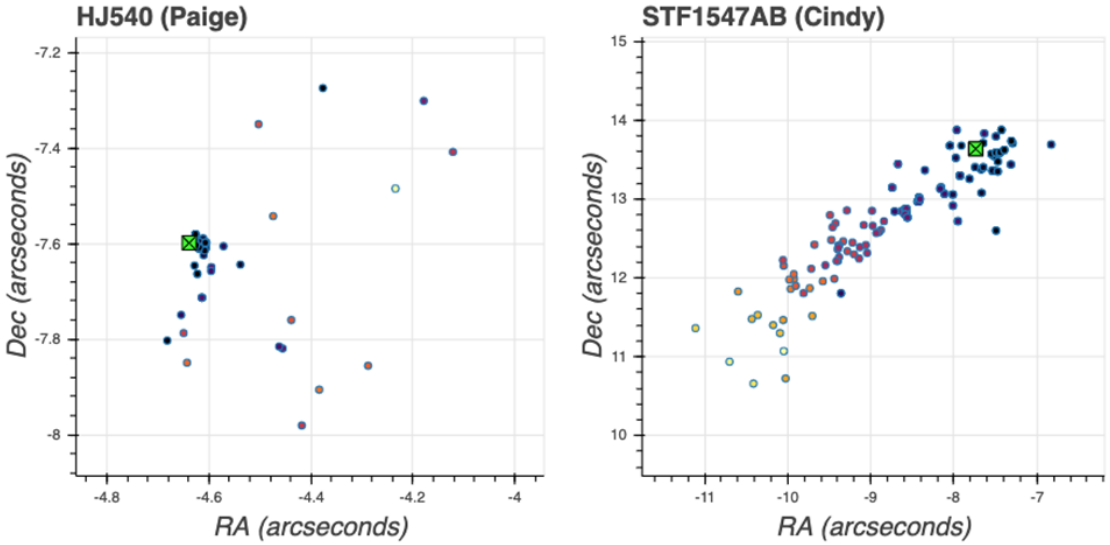

Figure 1 (conclusion). Measurements of each system in the context of historical data, with more recent measurements colored darker, and the measurement reported in this paper shown as a green square with an x through it.

Likelihood of a Gravitational Relationship

The similar parallax and common proper motion of these systems indicate that the component stars of each are likely to be related in some way. For example, they might share a common origin. Studying the trajectories of stars that were born together can help astronomers understand galactic structure on a larger scale. Even more importantly, some of the systems might be binary.

For most of these systems, a binary relationship between the components is not defendable on the basis of the historical data plots in Figure 1, because the scatter among the measurements is larger than the stars' relative motion over the time span of the plot. Since the data are colored chronologically in Figure 1, systems that exhibit consistent relative motion show a clear progression in shading from one side of the plot to the other. On the other hand, systems that do not show consistent relative motion over time will show darker points interspersed with lighter points, indicating that the stars' relative motion is smaller than the inherent uncertainty in the measurement.

For three of the systems, there was sufficient evidence of movement over time that it was appropriate to fit the data to assess the nature of the trend. These three cases were STF1547AB, STF443AB, and COU91AB. The first two of these have orbital solutions on file at the USNO, and these are shown in Figure 2. Note that STF1547AB's orbit has a grade of 5 while STF443AB's orbit has a grade of 4, indicating that STF1547AB's solution is considered the less cer-

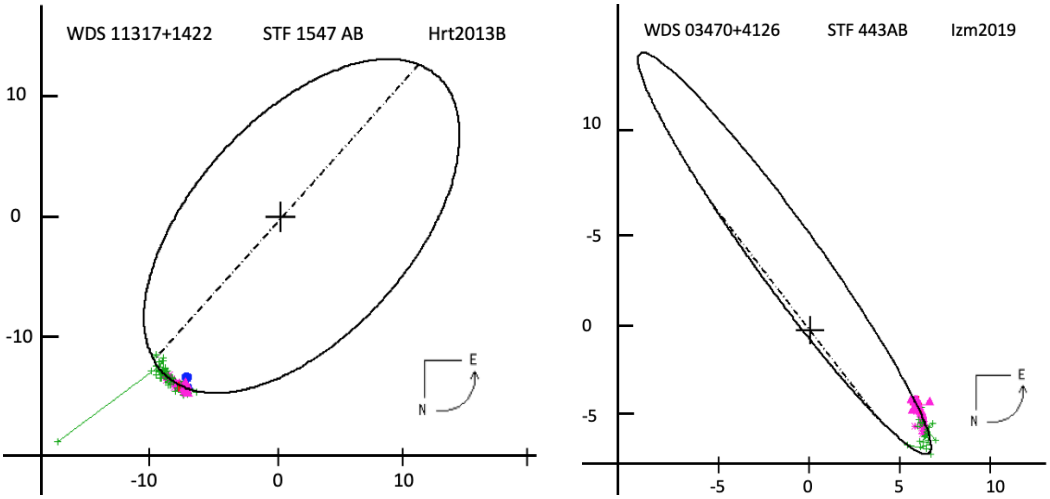

Figure 2. Existing orbital solutions for STF 1547AB (Grade 5) and STF 443AB (Grade 4).

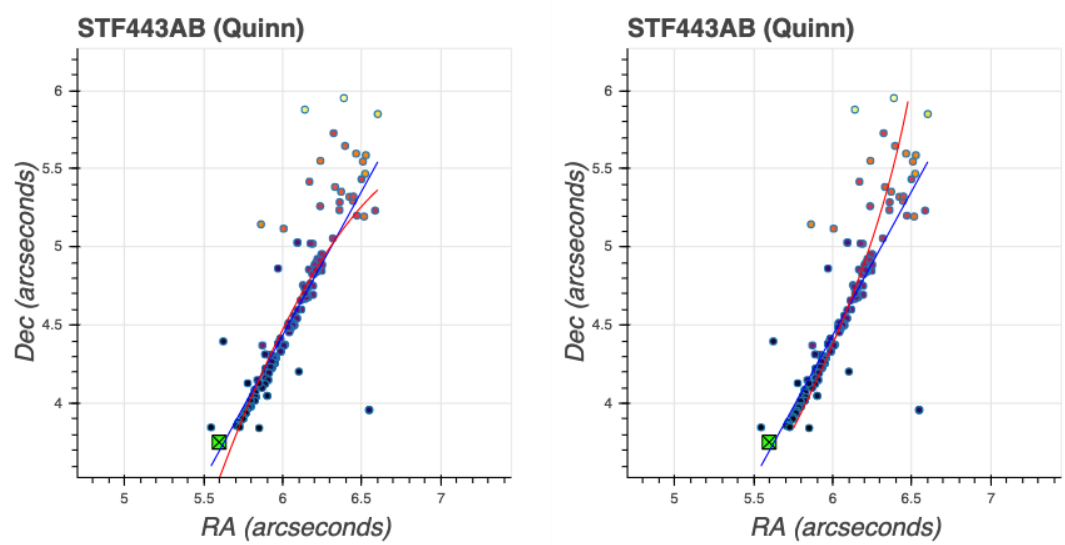

Figure 3: STF443AB weighted 2nd-order polynomial fits, showing a more realistic fit on the right when the axes of RA and Dec are switched. Both the linear and polynomial fits had R^2 ~= 0.7.

tain of the two. For COU91AB, an additional word of caution is appropriate, because the light-colored early measurement at the far left of the historical data plot might be causing the trend to seem more pronounced than it actually is. Therefore, any inferences about this system must be understood as especially preliminary.

Historical measurements for STF443AB, STF1547AB, and COU91AB were weighted according to a system developed by Richard Harshaw (Harshaw, 2020). The weighting criteria included measurement type, telescope aperture, and number of nights. After weighting, linear and second-order polynomial fits were performed. The purpose of these fits was to assess whether the seeming curve in the motion of the secondary with respect to the primary was more likely than the linear trend which would occur for unbound systems.

Sometimes, the fitting software produces inappropriate results when the historical measurements are close to perpendicular with respect to the axis of Right Ascension. This is because the fitting routine is looking for the best-fit parabola that has a unique y for every x, not the best-fit orbit. Figure 3 shows a case for which the 2nd-order polynomial fit of RA with respect to Dec yields a more reasonable result than a fit of Dec with respect to RA. This example illustrates the importance of selecting the vertical axis of the second-order fit to ensure that the fit makes sense in the context of the data, and to maximize the R2 value of the fit. For instance, a curve that does not have a possibility of enclosing the origin, where the primary star is located, would suggest no gravitational relationship between the stars. For each of the three systems, the orientation of the 2nd-order fit was selected according to these criteria. Still, none of the cases showed curvature sufficiently pronounced as to be definitive.

The chronological order of the points plotted on Figures 3 and 4 is displayed via the colormap, where lighter points correspond to measurements that were made earlier in time. The progression of the points from light to dark across each plot indicates the chronological trend.

Escape Velocities

In situations such as these, where historical measurements span an insufficient time period for a plot of past measurements to definitively characterize the system as binary, one metric that can be employed is the system's escape velocity. In order to calculate this, two numbers are needed: the mass of the primary star and the spatial separation of the stars. Once these numbers are obtained, the escape velocity can be calculated using Equation 1

$$v_{esc} = \sqrt{\frac{2GM}{r}} \qquad [1]$$

where M is the mass of the primary star and r is the separation of the primary and secondary in space.

If the secondary star is moving faster than escape velocity relative to the primary star, then the likelihood that the system is binary decreases, and vice versa. However, one caution is that both the relative velocity

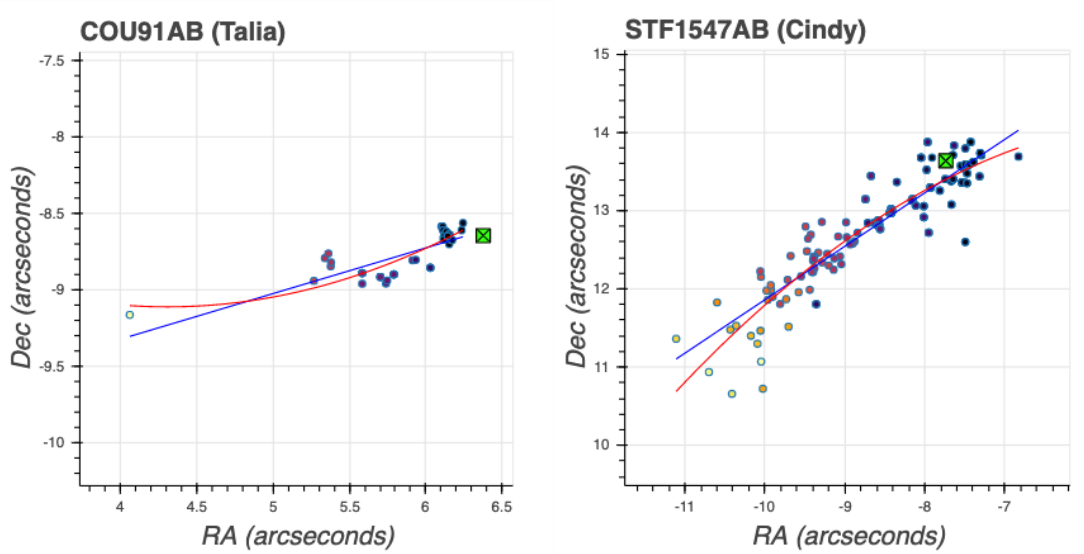

Figure 4. STF1547AB and COU91AB with weighted linear and 2nd-order polynomial fits. COU91AB's fits had R^2=0.616 (linear) and R^2 = 0.697 (polynomial). STF1547AB's fits had R^2 0.819 (linear) and R^2 = 0.831 (polynomial).

and the escape velocity are computed based on estimates that have large error bars.

To find the mass of the primary star, the star's spectral type was determined from its temperature listed in Gaia DR2. Its luminosity was also obtained from Gaia DR2 where available. For cases in which luminosity was not listed in Gaia DR2,missing, it was calculated from the magnitude and parallax of the star according to Equations 2 and 3.

$$M = m + 5\left(\log p + 1\right) \qquad [2]$$

where M is the absolute magnitude, m is the apparent magnitude, and p is the parallax.

$$\frac{L}{L_\odot} = 10^{0.4(4.85-M)} \qquad [3]$$

where L is the luminosity of the star, $L_\odot$ is a solar luminosity, and 4.84 is the absolute magnitude of the Sun.

The temperature and luminosity of the primary star were then used to locate it on a Hertzsprung-Russell (HR) diagram, where its position was used to verify that it was on the Main Sequence. All of the stars in this study had temperatures and luminosities consistent with Main Sequence stars. The HR diagram position was then used to estimate the mass of each primary. The spatial separation r of the primary and secondary stars was computed as the stars' transverse separation in radians divided by their parallax. The radial component of the stars' separation is not incorporated, because this value has an especially large associated error for the systems in this study. For most of these systems, the error on radial separation is almost as large or even larger than the radial separation itself. In other words, given the error on the corresponding parallax measurements, the stars in these systems might be exactly the same distance from Earth. Therefore, incorporating their separation in the radial dimension into r has the potential to artificially lower the computed system escape velocities. Because the separation of the stars was only considered in two dimensions, the escape velocities computed here should be considered to be an upper bound on the system escape velocity.

The velocity of the secondary star relative to the primary incorporated the stars' relative proper motions and their radial velocities, where available in Gaia DR2. Since radial velocities are listed in units of km/sec in Gaia DR2, the proper motions were converted from milliarcseconds per year to km/sec according to Equation 4,

$$\frac{mas}{yr}\cdot\frac{1''}{1000mas}\cdot\frac{1^\circ}{3600''}\cdot\frac{2\pi}{360^\circ}\cdot\left(\frac{1}{plx}\right)pc\cdot\frac{3.086\times10^{13}km}{pc}\cdot\frac{1yr}{3.54\times10^{7}s} \qquad [4]$$

(where the values from Gaia are in red) before computing the magnitude of the secondary motion vector subtracted from the primary.

System	Mass of Primary (solar masses)	Transverse separation in space (pc)	Upper Bound Escape velocity (m/s)	Relative 3D or 2D space velocity (m/s)
STF1188	1.21	0.0068	1234	1060*
STF 427	2.23	0.0053	1904	2556*
STF 872AB	1.73	0.0043	1550	1210*
STF 612AB	0.85	0.0023	1781	685
COU 91AB	0.45	0.0009	2160	2353*
STF1219	0.82	0.0030	1561	826
STF 1246	1.19	0.0043	1541	921
STT 195AB	1.55	0.0043	1759	4559
STF1050AB	2.33	0.0218	952	550*
STF1124AB	2.23	0.0319	627	1021*
STF 443AB	0.71	0.0008	154**	2239
STF1308	1.67	0.0064	1505	1884
STF1547AB	1.10	0.0018	2312	2007
HJ 540	1.48	0.0077	1289	782*

* Denotes a 2-d relative velocity if radial velocities are not available in Gaia DR2.

** For this system, 3-d spatial separation was used instead of transverse separation in the escape velocity calculation because the error on distance was not as large as for other systems in the study.

Table 3: Estimates of mass, spatial separation, relative velocity, and escape velocity.

Unlike radial separations, radial velocities are measured from Doppler shifts, and have a low associated error, which justifies their inclusion in the relative motion calculation. Where radial velocities are not available, the relative space velocity is two dimensional and should be considered a lower bound. The systems to which this applies are asterisked in Table 3.

Because they are estimated from so many imprecisely-known values, most of the escape velocities shown in Table 3 are not sufficiently different from the stars' relative velocities to base a definitive conclusion on their relative values. The escape velocities and relative velocities would need to differ by a factor of approximately 4 or 5 to support or challenge a conclusion regarding whether the system was gravitationally bound. Nevertheless, the numbers shown here can provide a rough estimate that might inform other pieces of evidence.

Conclusion

Measurements of 14 double star systems with similar parallax and proper motions are contributed here in the spirit of Brian Mason's call for observations (Mason, 2020). The systems we studied and measured are candidates for a physical relationship, making them important systems to follow over time. Continued observation and measurement of these and other double star systems is essential to our understanding of stellar motions and stellar orbits, which indirectly yields clues about galactic structure and stellar evolution.

Since its establishment in the late 1900's, the Washington Double Star Catalog has become continuously more valuable as measurements are added, making orbital solutions possible for increasingly long-period systems and characterizing the motions of increasingly slow-moving stars (Tenn, 2013). The measurements in this paper constitute our class's contribution to that ambitious project.

Acknowledgments

This research was made possible by the Washington Double Star catalog maintained by the U.S. Naval Observatory, the Stelledoppie catalog maintained by Gianluca Sordiglioni, Astrometry.net, AstroImageJ

software which was written by Karen Collins and John Kielkopf, and Stellarium software by Fabien Chéreau. This research also used data from the European Space Agency's Gaia Data Release 2 (https://www.cosmos.esa.int/gaia), processed by the Gaia Data Processing and Analysis Consortium (DPAC, https://www.cosmos.esa.int/web/gaia/dpac/consortium). Funding for the DPAC has been provided by national institutions, in particular, those participating in the Gaia Multilateral Agreement.

Special thanks to Richard Harshaw for his advice on our paper as well as developing and sharing the Plot Tool 3.18 that facilitated graphing the historical observations and weighting the data for the fits. Thanks also to Richard Harshaw and Rick Wasson for reviewing a draft of this paper and for making many valuable suggestions for improvement, which we have incorporated into this final version.

References

Caputo, Ryan, 2019, "The Human Element: Why Robotic Telescope Networks Are Not Always Better, and Performing Backyard Research", *Journal of Double Star Observations*, **15** (3), 408 - 415.

Harshaw, Richard, 2016, "CCD Measurements of 141 Proper Motion Stars: The Autumn 2015 Observing Program at the Brilliant Sky Observatory, Part 3", *Journal of Double Star Observations*, **12** (4), 394 - 399.

Harshaw, Richard, 2020. Private communication.

Luri, X., A. G. A. Brown, L. M. Sarro, F. Arenou, C. A. L. Bailer-Jones, A. Castro-Ginard, J. de Bruijne, T. Prusti, C. Babusiaux,, and H. E. Delgado. "Gaia Data Release 2: Using Gaia parallaxes", *Astronomy and Astrophysics*, **616**, A9, 1 - 19.

Mason, Brian, 2020, "Catalog Access and New Lists of Neglected Doubles", *Journal of Double Star Observations*, **16** (1), 3 - 4.

Tenn, Joseph, 2013. "Keepers of the Double Stars", *Journal of Astronomical History and Heritage*, **16** (1), 81 - 93.